Evolution of electronic structure with dimensionality in divalent nickelates

K. Maiti, Priya Mahadevan,* D. D. Sarma†
Solid State and Structural Chemistry Unit, Indian Institute of Science, Bangalore 560 012, India
(Received 12 August 1998)

We investigate the evolution of electronic structure with dimensionality (d) of Ni-O-Ni connectivity in divalent nickelates, NiO (3-d), La_2NiO_4, Pr_2NiO_4 (2-d), Y_2BaNiO_5 (1-d) and Lu_2BaNiO_5 (0-d), by analyzing the valence band and the Ni $2p$ core-level photoemission spectra in conjunction with detailed many-body calculations including full multiplet interactions. Experimental results exhibit a reduction in the intensity of correlation-induced satellite features with decreasing dimensionality. The calculations based on the cluster model, but evaluating both Ni $3d$ and O $2p$ related photoemission processes on the same footing, provide a consistent description of both valence-band and core-level spectra in terms of various interaction strengths. While the correlation-induced satellite features in NiO is dominated by poorly screened d^8 states as described in the existing literature, we find that the satellite features in the nickelates with lower dimensional Ni-O-Ni connectivity are in fact dominated by the *over-screened* $d^{10}\underline{L}^2$ states. It is found that the changing electronic structure with the dimensionality is primarily driven by two factors: (i) a suppression of the nonlocal contribution to screening; and (ii) a systematic decrease of the charge-transfer energy Δ driven by changes in the Madelung potential. [S0163-1829(99)09619-8]

I. INTRODUCTION

Electronic structure of transition metal oxides has been an active field of research for several decades arising from many puzzling issues such as the nature and origin of the insulating state in partially filled $3d$ systems, like NiO and the existence of metal-insulator transitions.[1] It is well known now that the electron-electron interaction effects play an important role in determining the electronic properties in these systems.[2] The interest in this particular class of compounds has seen an explosive growth in recent times due to the discovery of several exotic properties exhibited by transition metal oxides, such as the colossal negative magnetoresistance,[3] and high-temperature superconductivity.[4] Such results have indicated a close interplay between the electronic structure and the geometric structure in these compounds. For example, it is observed that while divalent three-dimensional copper oxide CuO is a wide band-gap insulator, essentially two-dimensional insulating La_2CuO_4 becomes superconducting upon hole doping.[5] Here, the dimensionality refers to the connectivity between the transition metal (TM) sites for the transport of charge carriers governed primarily by transition metal-oxygen-transition metal hopping interactions. A decrease in dimensionality is expected to reduce the bandwidth by affecting the effective coordination number for such electron transfers. Hence, the effective electron correlation is expected to increase with decreasing dimensionality of the system. However, the band gap in several systems are found to be less sensitive to the change in dimensionality. For example, the band gaps in three-dimensional cuprate CuO,[6] two-dimensional La_2CuO_4,[7] and one-dimensional Sr_2CuO_3[5] and Ca_2CuO_3[8] are about 1.4, 1.8, 1.5, and 1.8 eV, respectively, indicating that the band gap does not exhibit any systematic trend with dimensionality of the electronic structure. This is somewhat unexpected since the Cu-O bond distances, controlling the hopping interaction parameters, are similar in all these three compounds and the bandwidth W to a large extent is expected to be controlled by the dimensionality of the Cu-O-Cu network. This relative insensitivity of the band gaps between these compounds with different structural motifs may be driven by a concomitant change in the charge-transfer energy Δ.[5,9,10] It has been suggested[5] that the change in Δ, which more than compensates the reduction in the near-neighbor coordination number in determining the bandgap, may be driven by changes in the Madelung potential with dimensionality.

Electronic structure of transition metal compounds in general and late transition metal oxides in particular have been usually described within a finite cluster[11–13] or an impurity model[14] containing a single transition metal site. In recent times, it has, however, been found to be necessary to go beyond the single transition metal-site model in order to provide an accurate description of the electronic excitation spectra of three-dimensional Ni and Cu oxides,[15–19] suggesting the importance of impurity-impurity interactions in determining the electronic structure. While it is straightforward to anticipate that such TM-TM interactions via the intervening oxygen sites would be less dominant with decreasing dimensionality of the TM-O-TM network, there has been no investigation of the systematic changes in the electronic structure with dimensionality, so far. In order to obtain a more detailed understanding of the role of dimensionality in determining the electronic structure, we investigate a series of divalent nickelates with different dimensionalities of the Ni-O-Ni connectivity. The systems studied here are three-dimensional NiO, two-dimensional La_2NiO_4 and Pr_2NiO_4, one-dimensional Y_2BaNiO_5, and zero-dimensional Lu_2BaNiO_5. We provide a brief overview of the structure and physical properties of these systems in Sec. II. Section III and Sec. IV describe in detail the experimental and theoretical methodologies, respectively, used for the present study. The results and discussions are presented in Sec. V and conclusions in Sec. VI.

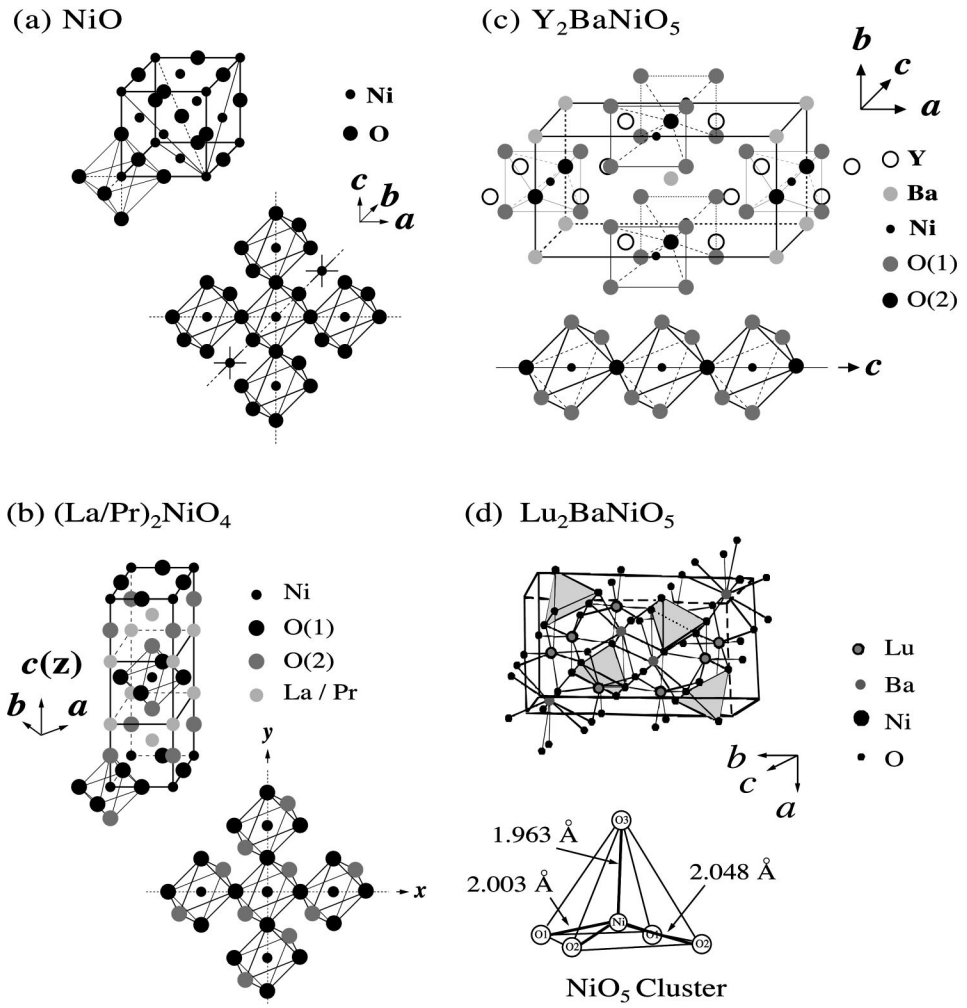

FIG. 1. The crystal structures and the typical Ni-O-Ni connectivities present in the structure shown for (a) NiO; (b) $(La/Pr)_2NiO_4$; (c) Y_2BaNiO_5; and (d) Lu_2BaNiO_5. The first three cases have corner shared NiO_6 octahedra extending in three, two, and one dimensions, respectively, while Lu_2BaNiO_5 has isolated NiO_5 clusters.

II. PREVIOUS WORK

NiO forms in the well-known rock-salt structure [Fig. 1(a)] with two interpenetrating fcc lattices of Ni and O. Ni-O bond length is 2.08 Å. Each Ni is surrounded by six oxygens forming a regular octahedron. The octahedra are connected to each other along all three (x, y, and z) directions by corner sharing with Ni-O-Ni bond angle of 180°. Thus, this system is an example of a three-dimensional network of Ni^{2+} in an octahedral crystal field of the oxygens. Optical measurements show the onset of absorption at about 4.3 eV,[20] which is consistent with the estimated bandgap from high-energy spectroscopic measurements.[21] Quantitative analysis of the valence-band spectra, which is dominated by the correlation effects have been carried out within the configuration interaction model for the NiO_6 cluster.[12,13] From these calculations it has been inferred that NiO is a charge-transfer insulator ($\Delta < U$) with a band gap of about 5 eV. The parametrized cluster analysis as well as analysis of calculations within the local-density approximation[12,13,22–24] have provided estimates of various electronic interaction strengths, such as the hopping interaction strengths, the charge-transfer energy, and the electron-electron multiplet interaction strengths. Besides certain approximations made within the cluster approach, which we discuss later in Sec. III in detail, these estimates from various approaches differ somewhat from each other. Moreover, the parameters estimated from valence band and the core-level spectra within the same cluster model are also slightly different.[12,13,24] Recently, it has been shown[15] that a proper description of the spectral shape of the $2p_{3/2}$ core-level photoemission observed in the experiments necessitates going beyond the single-cluster approach emphasizing the importance of nonlocal screening in determining the electronic structure of NiO.

The structure[25] of $La_2NiO_{4+\delta}$ is K_2NiF_4 derived [Fig. 1(b)]. The samples prepared in atmosphere ($\delta \sim 0.1$) possess tetragonal structure with Ni-O-Ni bond angle 180°. The lattice constants are $a = b = 5.4701$ Å and $c = 12.6401$ Å. The Ni atoms are surrounded by six oxygen atoms making a distorted octahedra with Ni-O bond lengths to be 1.9486 and 2.261 Å along and perpendicular to the Ni-O plane in the structure, respectively. These elongated octahedra are linked via the corner sharing of oxygen atoms along x and y directions and are well separated along z direction, as shown in Fig. 1(b). Thus, the electronic properties in this system are essentially controlled by the electronic structure of the two-

dimensional network of NiO_6 octahedra.[26] Kuiper *et al.*[27] observed a charge excitation gap of at least 4.0 eV in this system on the basis of oxygen *K*-edge x-ray absorption study. Electron energy-loss spectroscopy shows similar spectral features as in NiO suggesting similar charge excitation gap ($\sim$4.0 eV) in this system.[28] Electronic structure of La_2NiO_4 has been investigated extensively due to the similarity of its crystal structure with that of La_2CuO_4. Band structure calculations[29,30] as well as analysis of various high-energy spectroscopic data[28,31] have provided estimates of various interaction strengths. As in the case of NiO, the different sets of such estimates are somewhat varied.

Pr_2NiO_4 also possesses K_2NiF_4 derived structure with orthorhombic or tetragonal distortions depending on the oxygen nonstoichiometry.[32] Samples prepared in atmosphere have the oxygen content of about 4.09 with orthorhombic structure, which becomes tetragonal at 565 K. This system has slightly smaller lattice constants ($a=5.3965$ Å, $b=5.4538$ Å, and $c=12.434$ Å), compared to La_2NiO_4 due to the smaller radius of Pr^{3+} compared to La^{3+} (Ref. 32). The distorted NiO_6 octahedra are connected by corner sharing as in La_2NiO_4 along *x* and *y* directions. Thus, the electronic structure is dominated by interactions within the *ab*-plane, providing another example of a two-dimensional system with Ni-O-Ni bond-angle smaller ($\sim$160°) (Ref. 33) than that (180°) in La_2NiO_4. Although a smaller Ni-O bond length compared to La_2NiO_4 will tend to enhance the *pd* interaction strength in Pr_2NiO_4, the reduced Ni-O-Ni angle will suppress the Ni-O-Ni hopping interactions compensating the overall change in the bandwidth to some extent. Transport measurements[32] show activated behavior with activation energy for transport to be about 0.13 eV. An insulator to metal transition has been observed in this system at about 347 K ($\delta=0.09$).[32] There is no detailed analysis of the electronic structure reported for Pr_2NiO_4.

Y_2BaNiO_5 is orthorhombic[34] with Nd_2BaPtO_5 type structure as shown in Fig. 1(c). Here, the NiO_6 octahedra are connected by corner sharing along only *c*-direction [see lower panel of Fig. 1(c)]. The octahedra are compressed along the chain direction with bond length about 1.88 Å and the bond length perpendicular to the chain direction is about 2.18 Å. The temperature dependence of the charge transport shows activated behavior with an energy gap of about 0.6 eV.[35] This particular system has attracted considerable attention in recent times in view of the Haldane conjecture[36] suggesting a gapped spin excitation spectrum in a one-dimensional $S=1$ spin chain. Extensive experiments[37,38] have indeed established such a gap in the spin excitation spectrum of Y_2BaNiO_5. Thus, this system provides an ideal example of one-dimensional electronic structure. The electronic structure investigation based on photoemission measurements shows spectral signatures of a charge-transfer insulator.[39] However, there is no quantitative analysis of the electronic structure so far in the published literature.

A smaller rare earth Lu at the place of Y in this system changes the structure to a Sm_2BaCuO_5 type *Pbnm* structure, where each Ni atom is fivefold coordinated with a distorted square pyramidal geometry.[40] The lattice constants are $a=6.931$ Å, $b=12.109$ Å, and $c=5.634$ Å with four formula units in each unit cell. The structure of Lu_2BaNiO_5 is shown in Fig. 1(d). The NiO_5 units are shown by shaded regions in the figure. One NiO_5 unit with the appropriate bond lengths (1.963 Å, 2.003 Å, and 2.048 Å) is also shown separately in the figure. All the Ni-O bond lengths are smaller than that in NiO. It is clear from the figure that there is no Ni-O-Ni type connectivity between different NiO_5 units and thus, the electronic structure of this system is dominated by that of isolated NiO_5 clusters representing a zero-dimensional system. Physical properties and the electronic structure of this highly insulating compound have not been studied in any detail.

III. EXPERIMENT

Polycrystalline NiO, La_2NiO_4, Pr_2NiO_4, Y_2BaNiO_5, and Lu_2BaNiO_5 were prepared following the procedures reported in the literature.[25,32–34,40,41] All the samples were characterized by x-ray diffraction measurements. The NiO samples obtained in our preparations were green in color, indicating a proper oxygen stoichiometry; nonstoichiometric samples are known to be black. The oxygen stoichiometry of $La_2NiO_{4+\delta}$ and $Y_2BaNiO_{5+\delta}$ were estimated by the potentiometric titration and the nonstoichiometry (δ) was found to be 0.09 and 0.01, respectively. The nonstoichiometry in Pr_2NiO_4 prepared by the same method is reported to be about 0.09.[32]

X-ray photoemission spectroscopic measurements were carried out with monochromatized Al $K\alpha$ source and dual Mg $K\alpha$ and Al $K\alpha$ x-ray source in a VSW multipurpose spectrometer. The resolution in the measurements was 0.8 eV in each case. The base pressure during the measurements was in the range of 2×10^{-10} mbar. All the measurements were performed at room temperature, in order to minimize the charging effects from these highly insulating samples. The samples were cleaned *in situ* by intermittent scrapings with an alumina file between the measurements and the surface cleanliness was monitored by the shape of the O 1*s* feature and the total C 1*s* signals. In the case of highly insulating samples, the charging effect was neutralized using a low-energy electron flood gun and Mg $K\alpha$ radiation was used for the measurements. We adopt the NiO valence band spectrum from Kowalczyk *et al.*;[42] this earlier published result, while being consistent with the NiO valence-band spectrum recorded by us, has a considerably improved resolution (0.4 eV).

IV. THEORY

In order to calculate various photoemission spectra from these compounds, we consider the typical NiO_n clusters present in these systems. Thus, an octahedral NiO_6 cluster was considered for the case of NiO, while distorted (D_{4h} symmetry) NiO_6 clusters were taken for La_2NiO_4, Pr_2NiO_4, and Y_2BaNiO_5. Lu_2BaNiO_5 was represented by the NiO_5 cluster shown in Fig. 1(d). The photoemission spectra were calculated within a parametrized many-body multiband model including orbital dependent electron-electron (multiplet) interactions. The model Hamiltonian can be expressed as

$$H=\sum_{\alpha\sigma}\epsilon_{d\alpha}d^{\dagger}_{\alpha\sigma}d_{\alpha\sigma}+\sum_{i\sigma}\epsilon_{p}p^{\dagger}_{i\sigma}p_{i\sigma}+\sum_{\mu\sigma}\epsilon_{c}c^{\dagger}_{\mu\sigma}c_{\mu\sigma}$$
$$+\sum_{\alpha i,\sigma}[t^{\alpha i}_{dp}d^{\dagger}_{\alpha\sigma}p_{i\sigma}+\text{H.c.}]+\sum_{ij,\sigma}[t^{ij}_{pp}p^{\dagger}_{i\sigma}p_{j\sigma}+\text{H.c.}]$$
$$+\sum_{\alpha\beta\gamma\delta,\sigma_1\sigma_2\sigma_3\sigma_4}U^{\alpha\beta\gamma\delta}_{dd}d^{\dagger}_{\alpha\sigma_1}d^{\dagger}_{\beta\sigma_2}d_{\gamma\sigma_3}d_{\delta\sigma_4}$$
$$+\sum_{\alpha\beta\mu\nu,\sigma_1\sigma_2\sigma_3\sigma_4}U^{\alpha\beta\mu\nu}_{dc}d^{\dagger}_{\alpha\sigma_1}d_{\beta\sigma_2}c^{\dagger}_{\mu\sigma_3}c_{\nu\sigma_4}$$
$$+\sum_{\mu\nu,\sigma\sigma'}\zeta_{2p}\langle\mu|l.s|\nu\rangle c^{\dagger}_{\mu\sigma}c_{\nu\sigma'}. \quad (1)$$

The fermion operators $d^{\dagger}_{\alpha\sigma}$, $p^{\dagger}_{i\sigma}$, and $c^{\dagger}_{\mu\sigma}$ represent the creation of an electron in Ni $3d$, oxygen $2p$ and Ni $2p$ levels, respectively. The indices $\alpha-\delta$, $\mu-\nu$, and $i-j$ denote the Ni $3d$, Ni $2p$, and oxygen $2p$ orbitals, respectively. $U^{\alpha\beta\gamma\delta}_{dd}$ and $U^{\alpha\beta\mu\nu}_{dc}$ in the above Hamiltonian correspond to the multiplet interaction strengths between Ni $3d$ electrons and Ni $2p$–Ni $3d$ electrons, respectively. The multiplet interactions within the $3d$ manifold were expressed in terms of the Slater integrals F^0_{dd}, F^2_{dd}, and F^4_{dd} and those within the $2p$-$3d$ manifold were expressed in terms of F^0_{pd}, F^2_{pd}, G^1_{pd}, and G^3_{pd}. The values of the Slater integrals F^2_{dd}, F^4_{dd}, F^2_{pd}, G^1_{pd}, and G^3_{pd} were fixed at 80% of their atomic Hartree-Fock values for Ni[43,44] to account for the screening present in the solid.[44,45] The values of the monopole terms, F^0_{dd} and F^0_{pd} were fixed according to the relations

$$U_{dd}=F^0_{dd}-2/63[F^2_{dd}+F^4_{dd}], \quad (2)$$

$$U_{dc}=F^0_{pd}-(1/15)G^1_{pd}-(3/70)G^3_{pd}, \quad (3)$$

where the quantities U_{dd} and U_{dc} correspond to the multiplet averaged Coulomb interaction strengths.

The hopping interaction strengths ($t^{\alpha i}_{dp}$) between Ni $3d$ and oxygen $2p$ orbitals were expressed in terms of the Slater-Koster parameters[46] $(pd\sigma)$ and $(pd\pi)$, while the hopping interaction strengths between nearest-neighbor oxygens, t^{ij}_{pp} were expressed in terms of $(pp\sigma)$ and $(pp\pi)$. We fixed the ratio of $(pd\pi)/(pd\sigma)$ to be -0.5 in all the calculations. The values of $(pp\sigma)$ and $(pp\pi)$ were fixed to the estimations (0.6 and -0.15 eV, respectively) obtained earlier in the literature to describe the electronic structure of NiO in terms of cluster model and local-density approaches.[22,23] Most of the compounds studied here exhibit more than one Ni-O and O-O distances within the NiO_n clusters. As the hopping parameters scale with the distance, we assume a scaling of $r^{-3.5}$ for the pd interactions and r^{-2} for the pp interactions;[47] however, the results are not particularly sensitive to the variations in these dependences within reasonable limits, as explicitly checked by us for several cases. Thus, the number of adjustable hopping parameters was reduced to only one $(pd\sigma)$, which was obtained by simulating the spectrum of NiO. With this value fixed for NiO, the various $(pd\sigma)$ values for different Ni-O interactions in the other compounds were obtained by scaling with the corresponding Ni-O bond lengths.

The bare energies of Ni $3d$, Ni $2p$ and oxygen $2p$ orbitals are given by $\epsilon_{d\alpha}$, ϵ_c, and ϵ_p, respectively. The energies of the d orbitals are determined by the crystal-field splitting. For the octahedral case, the splitting between the t_{2g} and e_g orbitals, $10Dq$, was taken to be 0.5 eV. In the clusters with D_{4h} symmetry, the energies of the $3d$ orbitals were expressed in terms of $10Dq$, Ds, and Dt.[48] In the present calculations, we set $Ds=0.05$ and $Dt=0.005$ eV. The crystal-field effect for the NiO_5 cluster in Lu_2BaNiO_5 was approximated to be zero in the present calculations. The bare-energy difference between the TM d and the oxygen p orbitals ϵ_d-ϵ_p is governed by the charge-transfer energy Δ as

$$\Delta=E(d^9\underline{L}^1)-E(d^8)=\epsilon_d-\epsilon_p+8U_{dd}. \quad (4)$$

$E(d^m\underline{L}^n)$ represents the degeneracy weighted multiplet average energy of the $d^m\underline{L}^n$ multiplets, L denoting a ligand hole state. In the final state of the core-level calculations, however, the corresponding energy Δ' is given by

$$\Delta'=E(\underline{2p}d^9\underline{L}^1)-E(\underline{2p}d^8)=\Delta-U_{dc} \quad (5)$$

due to the presence of the core hole.

It is well known that parametrized model Hamiltonian approaches often lead to nonunique solutions due to the presence of a large number of parameters; thus, it is highly desirable to constrain the parameter values from other physical considerations. As already pointed out, we expect the hopping interaction strengths to be transferable from one compound to another by scaling the Slater-Koster parameters, $(pd\sigma)$, $(pd\pi)$, $(pp\sigma)$, and $(pp\pi)$ by the Ni-O and O-O distances. Moreover, the multiplet interaction parameters, F^2_{dd}, F^4_{dd}, F^2_{pd}, G^1_{pd}, and G^3_{pd} are also expected to remain the same between the various divalent Ni oxides; thus, these parameters were fixed at 80% of their atomic Hartree-Fock values, according to the usual practice. This leaves us with only three parameters, namely, F^0_{dd}, F^0_{pd}, and Δ, to simulate the spectral features of the four compounds discussed here. The freedom to choose the parameter values were further curtailed by requiring that F^0_{dd} value be the same for all four compounds. Thus, we have tried to simulate the spectral features in the four compounds by adjusting the values of two interaction strengths only, namely F^0_{pd} and Δ. We believe that this procedure of minimizing the number of adjustable parameters is important to obtain reliable estimates of the interaction strengths. Moreover, the calculated spectra are not equally sensitive to the variations in the interaction parameters; thus, it has been generally found that the accuracies of various quantities extracted from such analysis of electron spectroscopic data are about ±0.2, ±0.5, and ±1 eV for the hopping interaction, charge-transfer energy, and the core-valence Coulomb interaction strengths, respectively. The reliability of the extracted parameters can be further enhanced by analyzing different spectral functions within the same model, as has been done in the present paper for core-level *and* valence-band spectra. Our results show that the accuracies of estimates for the two adjustable parameters Δ and F^0_{pd} are about ±0.3 and ±0.8 eV, respectively; calculated spectra with Δ and F^0_{pd} outside this limit of the optimal choice yields distinguishably poorer simulations of the experimental data.

The usual practice of analyzing the valence-band spectra of transition metal oxides within similar many-body approaches has been to calculate the transition metal $3d$ component of the valence-band photoemission within such models, while approximating the oxygen $2p$ component by a Gaussian function. This allows the oxygen $2p$ component to have any energy most suited to simulate the experimental spectra. This does not pose a serious limitation in cases like NiO and CuO, since the valence-band photoemission of such compounds is dominated by the transition metal $3d$ contributions, arising from the equal atomic distribution between the metal and the oxygen, and a much larger photoemission cross section for the $3d$ states. However, the compounds investigated here with oxygen to nickel ratio as high as 5:1, the valence-band spectra are significantly contributed by the oxygen p-derived states, requiring a more unambiguous approach to estimating this contribution. It is to be noted here that the model described above also determines the oxygen p contribution to the photoemission spectra and it is straightforward to calculate this component in exactly the same way as that for the Ni d contributions. Thus, the spectral function corresponding to oxygen p photoemission contributions in the valence-band spectrum was also calculated under the same parametrization for the results presented here.

The calculation of the spectral function has been performed using Lanczos algorithm.[49] The calculated photoemission spectra were convoluted with a Lorentzian having an energy dependent full width at half maximum (FWHM), in order to account for the lifetime effects. The energy dependence was considered to be linear following the earlier literature,[12,13,50,51] $\Gamma(\epsilon)=\Gamma_0+\alpha\times(\epsilon-\epsilon_0)$, where $\Gamma(\epsilon)$ is the half-width at half maximum of the Lorentzian to be convoluted at the energy ϵ, Γ_0 is a constant, and ϵ_0 is the energy of the lowest-energy feature in the spectrum. For the core-level spectra we used $\Gamma_0=0.2$ eV and α in the range of 0.1–0.18. In the case of valence-band spectra, the value of α used was 0.1 and $\Gamma_0=0.15$ eV in every case. Other broadening effects, such as the spectrometer resolution function, broadening due to solid state effects, were introduced by convoluting the lifetime broadened spectra with a Gaussian function. In order to simulate the Ni $2p$ core-level spectra the Gaussian broadening used are 3.3 eV FWHM in the case of three-dimensional NiO and 2 eV in the lower dimensions. It is to be noted that the Gaussian broadenings used here are substantially larger than the width ($\approx$0.8 eV) of the resolution function of the present experiments. This need for an extra broadening for the core-level spectra is well known in the literature and possibly arises from various solid-state effects, such as the phonons, oxygen bandwidth, and nonlocal screening channels, not included in the NiO_n cluster model considered here. While the phonon contribution is expected to be not very large, the other two effects can contribute significantly. The main peak in the core region arises primarily from a charge-transferred state $d^9\underline{L}^1$. The hole in the ligand ($\underline{L}^1$) can be at any energy over the entire bandwidth of the oxygen p band in a real solid, giving a spectrum of possible energies for the $d^9\underline{L}^1$ configurations. On the other hand, in the model approach, this has a well-defined energy due to the neglect of the oxygen p bandwidth. Thus, it becomes necessary to broaden the calculated spectrum beyond the resolution and lifetime effects in order to account for the neglect of the oxygen bandwidth in the model Hamiltonian approach. Additionally, nonlocal screening channels have been shown to contribute a significant broadening in the three-dimensional case.[15] This possibly explains the extra broadening needed for the three-dimensional NiO compared to the other compounds.

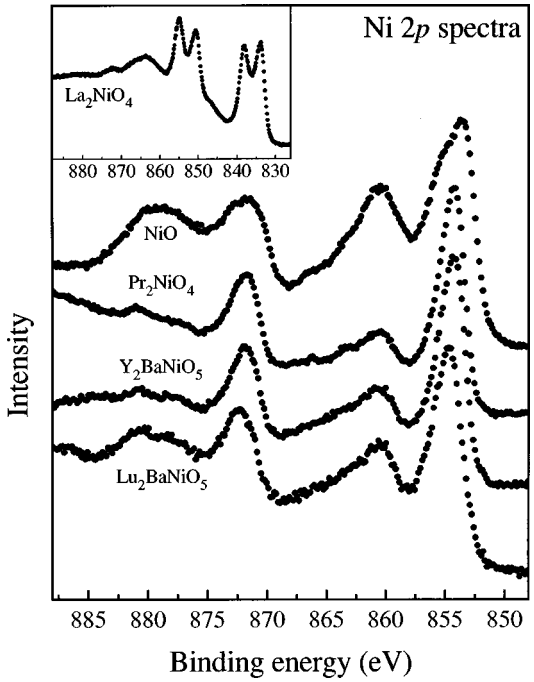

FIG. 2. Ni $2p$ core-level spectra of NiO, Pr_2NiO_4, Y_2BaNiO_5, and Lu_2BaNiO_5. The inset shows the Ni $2p$ and La $3d$ spectral region in La_2NiO_4. This spectrum is dominated by the La $3d$ derived signals.

The width of the corresponding Gaussian functions for the $3d$ components in the valence-band spectra was 1.2 eV for La_2NiO_4 and Y_2BaNiO_5, and 0.8 eV for NiO. The oxygen $2p$ contribution in the valence-band spectrum was convoluted with a Gaussian with larger widths ($\sim$2 times) in order to simulate the total spectrum; this may arise from the fact that the smallest clusters considered here have half of the nearest-neighbor oxygen sites missing. It is known[52] that the photoemission cross section for the oxygen $2p$-like states is much smaller compared to the cross section of the Ni $3d$-like states at the energy of Al $K\alpha$ radiation. This was taken into account by considering about 25% of the calculated oxygen $2p$ intensity compared to that of the Ni $3d$ contributions, which is about six times larger than the photoemission cross section calculated for the atomic cases. Such an intensity ratio has indeed been used earlier in the literature in order to obtain the total intensity of the photoemission spectra[12,28] and is possibly related to the oxygen-oxygen and oxygen-transition metal interactions in the solid.[53] The inelastic background present in the experimental spectrum has been accounted for by adding an integral background to the calculated spectrum.

V. RESULTS AND DISCUSSION

We show the Ni $2p$ core-level spectra of NiO, Pr_2NiO_4, Y_2BaNiO_5, and Lu_2BaNiO_5 in Fig. 2 with the corresponding

spectrum of La_2NiO_4 shown in the inset. In the inset, it is observed that the La $3d$ signals overlap with Ni $2p$ signals extensively in La_2NiO_4, precluding any analysis of the electronic structure on the basis of the core-level spectrum in this case. Thus, we use Pr_2NiO_4 for analyzing the electronic structure of two-dimensional nickelates from the core-level spectrum. There are four dominant features in each of the spectra shown in the main frame of the figure. The intense peaks in the energy ranges 850–858 eV and 868–875 eV binding energies are due to Ni $2p_{3/2}$ and $2p_{1/2}$ spin-orbit split signals, respectively. These signals are known to arise from the charge transferred well-screened final states in the case of NiO[12,13] and La_2NiO_4.[28] In addition to these, the strong intensity features in the energy ranges 858–868 eV and 875–886 eV are the so-called satellites accompanying the $2p_{3/2}$ and $2p_{1/2}$ main lines, respectively. These features are known to arise essentially due to the unscreened or poorly screened d^8 contributions in the final state. The main $2p_{3/2}$ and $2p_{1/2}$ signals of NiO appear distinctly broader than the corresponding signals from the other compounds; the $2p_{3/2}$ spectral shape in particular suggests the existence of two features in the main line for NiO, the lowest energy main peak at about 853.5 eV binding energy with a shoulder at about 854.8 eV binding energy. It is interesting to note that such distinct two featured spectral shape are not present in the spectra of other compounds shown in Fig. 2; both $2p_{3/2}$ and $2p_{1/2}$ main spectral features are significantly narrower in these compounds compared to those in NiO. Moreover, the main peak positions in these compounds (Pr_2NiO_4, Y_2BaNiO_5, and Lu_2BaNiO_5) appear closer to the spectral feature appearing as the shoulder at about 854.8 eV in NiO. Interestingly, in the zero-dimensional system Lu_2BaNiO_5, the $2p_{3/2}$ main peak appears exactly at the energy position corresponding to the shoulder in the main peak of NiO (Fig. 2). This conclusively shows that the spectral feature at the higher binding energy of about 854.8 eV arises from screening dynamics within the local NiO_n cluster, which is the only screening channel available for the zero-dimensional compound with its isolated clusters. The main peak in NiO, whose contribution decreases with decreasing Ni-O-Ni connectivity and vanishes altogether for the isolated cluster compound, is then identified as arising from nonlocal screening channels as observed in cuprates.[54] This provides an experimental verification of the earlier theoretical predictions in the case of NiO[15] where the calculations were performed to establish the nonlocal nature of the screening responsible for the main peak within a multi-impurity model. In the case of three-dimensional network of NiO, it is necessary to consider six neighboring Ni sites connected to the central Ni site via Ni-O-Ni hopping. Such a many-body calculation becomes prohibitively large and it was necessary to make use of certain simplifying approximations.[15] It is to be noted that in contrast, the two-dimensional and one-dimensional compounds discussed here have only four and two neighboring Ni sites. This should enable the theoreticians to perform more complete analysis without any further approximations within the multi-impurity model. Thus, the present results provide a suitable ground for testing the nature and origin of the nonlocal screening dynamics more rigorously, though such calculations are outside the scope of the present paper.

The satellite feature associated with the Ni $2p_{3/2}$ spectral region also exhibits substantial changes with dimensionality. The intensity of the satellite features in the compounds with lower dimensionality is significantly lower compared to that for three-dimensional NiO. This is somewhat surprising in view of the fact that a lower-dimensional system is expected to have a lower bandwidth and consequently, a higher correlation effect; an enhancement of the correlation effect normally increases the intensity of the satellite in contrast to the observed experimental trend. Thus, it suggests that there must be a compensating change in another electronic interaction strength opposing the influence on the satellite intensity arising from decreased possibility of the delocalization in the reduced dimensionality. Detailed analysis of the spectral shape suggests this compensating change is a systematic lowering of the charge-transfer energy Δ with decreasing dimensionality, as discussed next.

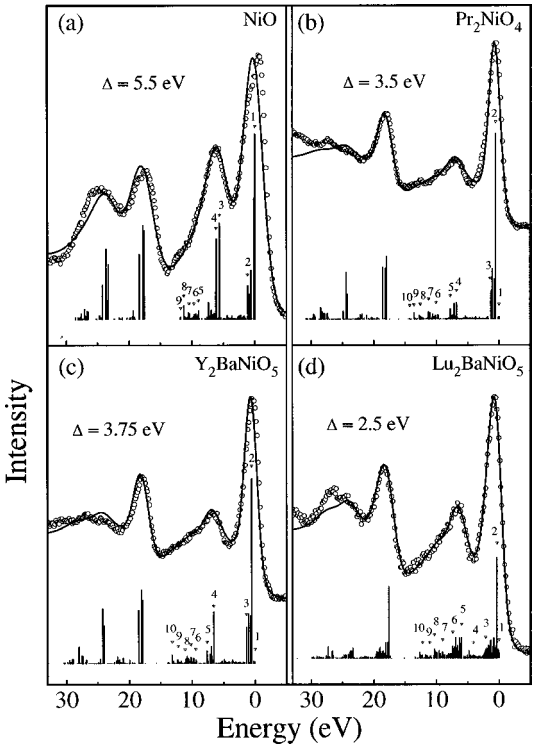

FIG. 3. Comparison of the experimental (open circles) and the calculated (thick lines) Ni $2p$ spectra for (a) NiO; (b) Pr_2NiO_4; (c) Y_2BaNiO_5; and (d) Lu_2BaNiO_5. The corresponding bar diagrams obtained from the cluster calculations are also shown. The numbers mark the energies where an analysis of the character of the final-state wave functions were carried out and the corresponding results are given in Tables I–IV.

In order to obtain a quantitative description of the electronic structure in these compounds, we have calculated the Ni $2p$ core-level spectra within the single-transition metal cluster approach. The resulting calculated spectra are shown by the solid lines in comparison to the experimental spectra (open circles) in Fig. 3. The calculated spectra without various broadenings are represented by the bar diagrams. The spectrum of NiO [see Fig. 3(a)] can be well described with $(pd\sigma) = -1.25$ eV, $\Delta = 5.5$ eV, $F^0_{dd} = 7.0$ eV, and $F^0_{pd} = 9.2$ eV. This value of F^0_{pd} coupled with the values of G's representing the multiplet interactions between the Ni $2p$ and $3d$ states yields a multiplet averaged value of the Cou-

TABLE I. Contributions of various configurations in the final states of the Ni $2p$ core-level photoemission in NiO.

Peak no.	1	2	3	4	5	6	7	8	9
Energy	0.0	1.12	5.63	6.47	8.97	9.70	10.42	11.29	11.84
d^8	20.20	10.21	59.09	45.40	17.83	21.61	50.08	69.12	77.38
$d^9\underline{L}$	65.07	72.51	9.54	30.61	29.65	22.76	26.62	21.54	16.87
$d^{10}\underline{L}^2$	12.73	17.28	31.37	23.99	52.52	55.63	23.30	9.33	5.75

lomb interaction strength, U_{dc} to be about 8.8 eV. The F^0_{dd} along with F^2_{dd} and F^4_{dd} chosen from the Hartree-Fock calculations gives the multiplet averaged value U_{dd}, of the Coulomb interaction strength between Ni $3d$ electrons to be 6.53 eV, which is in good agreement with an earlier estimate[24] of 6.86 eV, while it is smaller than another estimate[12] of 8 eV. The calculated spectrum (solid line) overlapped with the experimental one (open circles) in Fig. 3(a) suggests a good agreement between the two, particularly in the region of $2p_{3/2}$ satellite structure. However, the main peak in the calculated spectrum consists of only one discernible feature appearing at the same energy as the shoulder of the main signal in the experimental spectrum. This is not surprising since this calculation employing a NiO_6 cluster does not include the effect of delocalization of the holes from the cluster via an additional screening channel involving the neighboring Ni sites; therefore, the present method cannot account for nonlocal screening effects,[15] responsible for the main peak in NiO as discussed earlier. The comparison of the calculated and the experimental spectra in the energy region of the $2p_{1/2}$ main signal exhibits similar agreement and discrepancy, as in the $2p_{3/2}$ case arising from the neglect of nonlocal screening effects in the theoretical model. In contrast to the case of $2p_{3/2}$ related photoemission spectrum, the observed spectral shape in the satellite region of the $2p_{1/2}$ signal is not simulated well by the calculation. It has been shown[55] that a strong interference of the near-threshold Coster-Kronig decay channels in the case of $2p_{1/2}$ photoemission of transition metal compounds substantially modifies the spectra. Thus, the disagreement observed between the calculated and experimental $2p_{1/2}$ satellite structure is possibly related to such extra decay channels for this core-hole state, not included in the present model.

The comparison between the calculation and the experiment as depicted in Fig. 3(a) suggests that a quantitative description of the electronic structure of NiO can be provided on the basis of present estimates of the various parameter strengths. On this basis, the ground-state wave function is found to contain 84.8%, 14.9%, and 0.3% of d^8, $d^9\underline{L}^1$ and $d^{10}\underline{L}^2$ configurations, respectively. This suggests an average $3d$ occupancy, n_d, of 8.16 which, based on the past experience,[56,57] is expected to be a reliable estimate. Thus, the ground state of NiO is characterized by substantial covalency effects in spite of large values of U_{dd} and Δ. Interestingly, this estimate is close to the value (8.2) obtained from neutron diffraction measurements.[58] Earlier analysis of NiO electron spectroscopic data obtained n_d to be 8.22 (Ref. 12) or 8.18 (Ref. 24). In order to understand the nature of the final states responsible for various features in the core-level spectrum [energy positions marked 1–9 in Fig. 3(a)] contributions of various configurations (d^8, $d^9\underline{L}^1$, and $d^{10}\underline{L}^2$) in the corresponding final-state wave functions are listed in Table I. It is clear from the table that the main signal arising from features in energy regions 1 and 2 is predominantly contributed by the charge transferred state ($d^9\underline{L}^1$), representing a state where the core hole is well-screened by the transfer of an electron from the ligand levels to the Ni $3d$ levels. The main satellite intensity arises from states with primarily unscreened d^8 character (marked 3 and 4). Higher energy, lower intensity features within the satellite region are contributed by states dominated by $d^{10}\underline{L}^2$ configurations (marked 5 and 6) as well as by states with dominant d^8 configurations [marked 7–9 in Fig. 3(a)]. It is to be noted that the $d^9\underline{L}^1$ configuration has the lowest energy in presence of the Ni $2p$ core hole, while d^8 and $d^{10}\underline{L}^2$ configurations are about 3.3 and 3.2 eV above the $d^9\underline{L}^1$ configuration, respectively. This explains why the lowest energy peak (the main signal) in the Ni $2p$ spectrum is dominated by $d^9\underline{L}^1$ configurations, while the satellite feature is contributed by both d^8 and $d^{10}\underline{L}^2$ configurations.

We compare the Ni $2p$ calculated core-level spectrum (solid line) for Pr_2NiO_4 with the experimental one (open circles) in Fig. 3(b). We have used the same parameter (F^0_{dd}, F^2_{dd}, F^4_{dd}, F^0_{pd}, F^2_{pd}, G^1_{pd}, and G^3_{pd}) values for the multiplet interactions as in the case of NiO. It turns out that the core-level spectrum of Pr_2NiO_4 can be simulated quite well by changing only the charge-transfer energy from $\Delta = 5.5$ eV for NiO to $\Delta = 3.5$ eV. The resulting calculated spectrum is compared with the experimental one in Fig. 3(b), exhibiting a good agreement. It is interesting to note that in this case, the calculation within the cluster model with a single transition metal ion provides a more satisfactory description of the main peak region indicating a considerably reduced influence of nonlocal screening contributions for the two-dimensional Pr_2NiO_4, in contrast to the three-dimensional NiO. Besides the role of dimensionality in determining the efficiency of the nonlocal screening channels, another contributing factor in suppressing this screening mechanism may be the presence of smaller Ni-O-Ni angle[33] in Pr_2NiO_4 compared to that in NiO. This results in a further reduction in the probability of hole delocalization in Pr_2NiO_4. An analysis of the ground-state wave function shows 74%, 25%, and 1% of d^8, $d^9\underline{L}^1$, and $d^{10}\underline{L}^2$ characters, respectively. This corresponds to an average $3d$ occupancy, n_d, of 8.27. An increased value of n_d in Pr_2NiO_4 compared to NiO indicates an enhanced effect of covalency in Pr_2NiO_4, arising from a significant decrease in Δ. Contributions of various electronic configurations (d^8, $d^9\underline{L}^1$, and $d^{10}\underline{L}^2$) to the final state wave functions corresponding to features marked 1–10 in Fig. 3(b) are listed in

TABLE II. Contributions of various configurations in the final states of the Ni $2p$ core-level photoemission in Pr_2NiO_4.

Peak no.	1	2	3	4	5	6	7	8	9	10
Energy	0.0	0.57	1.3	6.8	7.82	10.10	11.26	12.57	13.59	14.30
d^8	8.64	13.12	6.74	32.03	18.60	40.35	65.73	78.32	83.51	84.56
$d^9\underline{L}$	63.00	63.74	63.91	20.25	20.95	30.59	24.11	17.87	14.37	13.53
$d^{10}\underline{L}^2$	27.18	23.14	29.35	47.72	52.45	29.06	10.16	3.81	2.12	1.91

Table II. Once again we find that the main peak has primarily well-screened $d^9\underline{L}^1$ character, as in the case of NiO. However, the character of the leading features (marked 4 and 5) in the case of Pr_2NiO_4 is dominated by $d^{10}\underline{L}^2$ configuration, in contrast to the case of NiO with its dominant d^8 character in this energy range. This implies that while the predominant character of the leading satellite intensity in NiO is the ''poorly screened'' d^8 state as reported earlier,[12] the same satellite spectral region in Pr_2NiO_4 has to be interpreted as an overcompensated screening or ''over-screened'' $d^{10}\underline{L}^2$ state with two charge-transfered electrons screening one core hole, in contrast to the usual interpretation. This surprising fact follows from the energetics of different electron configurations arising from a change in Δ between NiO and Pr_2NiO_4. While, in presence of the core-hole $d^9\underline{L}^1$ configuration still has the lowest energy, the energies of d^8 and $d^{10}\underline{L}^2$ states are 5.3 and 1.2 eV, respectively, with respect to the $d^9\underline{L}^1$ state in Pr_2NiO_4. This energy ordering is responsible for making the $d^{10}\underline{L}^2$ state contribute dominantly in the leading satellite features of Pr_2NiO_4. The higher-energy spectral region within the satellite feature, marked 6–10 in Fig. 3(b), is, however, dominated by d^8 contributions (see Table II).

We show the calculated Ni $2p$ core-level spectrum (solid line) for Y_2BaNiO_5 in comparision to the experimental one (open circles) in Fig. 3(c). The calculated spectrum in this case was obtained for $\Delta=3.75$ eV and $U_{dc}=8.6$ eV (corresponding to $F^0_{pd}=9.0$ eV), while keeping all other parameters the same as in the case of NiO and Pr_2NiO_4. While the Δ value for this one-dimensional nickelate is marginally larger than that ($=3.5$ eV) in the two-dimensional Pr_2NiO_4, it is substantially smaller than the Δ ($=5.5$ eV) in three-dimensional NiO. The ground-state wave function for this parameter set contains approximately 76%, 23%, and 1% of the d^8, $d^9\underline{L}^1$, and $d^{10}\underline{L}^2$ configurations, respectively. The average number of $3d$ electrons, n_d is 8.24 in this case. The characters of the wave functions in the final states are given in Table III, with the corresponding energies marked 1–10 in the figure. These characters, in terms of the well-screened $d^9\underline{L}^1$, poorly screened d^8, and over-screened $d^{10}\underline{L}^2$ configurations are similar between Pr_2NiO_4 and Y_2BaNiO_5, due to their similar Δ values. Thus, the main peak arises due to the well-screened $d^9\underline{L}^1$ state and the leading features in the satellite are primarily due to overscreened $d^{10}\underline{L}^2$ configurations with the poorly screened d^8 states contributing significantly to the higher-energy region within the satellite structure.

In order to obtain the parameter values for the zero-dimensional case, we have calculated the Ni $2p$ core level spectrum for Lu_2BaNiO_5. The calculation considers the actual bond lengths in the NiO_5 cluster of this compound. The experimental and the calculated spectra are plotted in Fig. 3(d), with $\Delta=2.5$ eV and $U_{dc}=7.3$ eV ($F^0_{pd}=7.7$ eV). It is evident from the figure that the calculated spectrum describes the experimental one very well. Such good agreement with the results of a single NiO_5 cluster calculation is indeed to be expected, since the NiO_5 units in this compound are isolated in the lattice leading to a negligible interaction between one cluster and another; thus, the cluster approximation becomes nearly exact for the charge dynamics in this system and the calculated spectrum provides a reliable description of the experimental spectrum up to about 24 eV. The mismatch beyond this energy region within the $2p_{1/2}$ satellite is possibly due to the presence of Coster-Kronig decay channels[55] as discussed in the case of NiO. The decrease of the U_{dc} value in this compound compared to those in NiO, Pr_2NiO_4, and Y_2BaNiO_5 is possibly related to the fact that the bond lengths are considerably smaller for all the Ni-O bonds in this zero-dimensional compound, giving rise to more efficient screening of the core hole due to extra-atomic relaxations. The ground-state wave function for Lu_2BaNiO_5 has 71%, 28%, and 1% of d^8, $d^9\underline{L}^1$, and $d^{10}\underline{L}^2$ configurations. Thus, the total $3d$ count is 8.3, which is the highest value of n_d among all the compounds investigated here. This is evidently related to the lowest Δ value leading to the largest covalency effect. The characters of final states are listed in Table IV, with corresponding features marked

TABLE III. Contributions of various configurations in the final states of the Ni $2p$ core-level photoemission in Y_2BaNiO_5.

Peak no.	1	2	3	4	5	6	7	8	9	10
Energy	0.0	0.53	1.35	6.58	7.65	9.44	10.19	11.13	12.25	13.23
d^8	9.02	12.86	7.30	33.08	17.52	34.37	57.02	73.11	81.07	85.00
$d^9\underline{L}$	64.58	64.37	65.12	16.50	27.72	27.62	26.84	20.20	15.81	13.06
$d^{10}\underline{L}^2$	24.40	22.77	27.58	50.41	54.76	38.02	16.14	6.69	3.12	1.94

TABLE IV. Contributions of various configurations in the final states of the Ni $2p$ core-level photoemission in Lu_2BaNiO_5.

Peak no.	1	2	3	4	5	6	7	8	9	10
Energy	0.0	0.34	2.13	4.09	5.98	7.40	8.99	10.46	11.06	12.19
d^8	7.29	9.34	3.95	2.51	18.30	14.33	41.09	70.51	80.03	84.64
$d^9\underline{L}$	63.50	63.33	66.59	82.33	25.99	26.30	32.54	22.84	16.36	13.50
$d^{10}\underline{L}^2$	29.21	27.33	29.46	15.15	55.70	59.38	26.37	6.65	3.61	1.86

1–10 in Fig. 3(d). The character of various features are again similar with those in one- and two-dimensions, with the leading energy features in the satellite region being more markedly over-screened in nature arising from further reduction of Δ and consequently, a greater stabilization of the $d^{10}\underline{L}^2$ over-screened configuration compared to the poorly screened configuration.

The above results show that the Ni $2p$ spectra of the divalent nickelates in various dimensions are well described within the cluster approximation. In order to establish the sensitivity of the calculated spectra on the various interaction strengths, thereby obtaining estimates of errors in evaluating these strengths from the comparison of experimental and calculated spectra, we show the effect of the change of various parameters in the calculated spectrum in Fig. 4, taking the case of zero-dimensional system as an example. The solid line represents the calculated spectrum for the optimum parameter set, discussed before. An increase only in Δ from 2.5 to 3.0 eV (dotted line in the figure) leads to an increase in the intensity of the overscreened states compared to the intensity of the poorly screened states within the satellite region. In contrast, an increase in the electron-electron interaction strength by 0.8 eV ($F^0_{pd}=8.5$ eV) between the core and valence electrons (dot-dashed line) enhances the intensity of the poorly screened states relative to the intensity of the over-screened states within the satellite features. Such changes are not surprising since the increase in F^0_{pd} increases the stabilization of the electrons in the Ni $3d$ levels in the final states due to increased attraction between the core hole and valence electrons. The separation between the main signal and the satellite feature is found to increase with the increase of 0.2 eV in the value of $pd\sigma$ ($=-1.5$ eV) along with a reduction in the satellite intensity (dashed line). It is thus obvious from the figure that the errors in estimating various parameter values are less than 0.5 eV for Δ, 0.2 eV for $pd\sigma$, and 0.8 eV for F^0_{pd}.

The valence-band spectra of all the compounds are shown in Fig. 5. The main frame of the figure contains the valence-band spectra of three-dimensional NiO, two-dimensional La_2NiO_4, and one-dimensional Y_2BaNiO_5. The spectra corresponding to Pr_2NiO_4 (two-dimensional) and Lu_2BaNiO_5 (zero-dimensional) are shown in the inset of the figure. It is

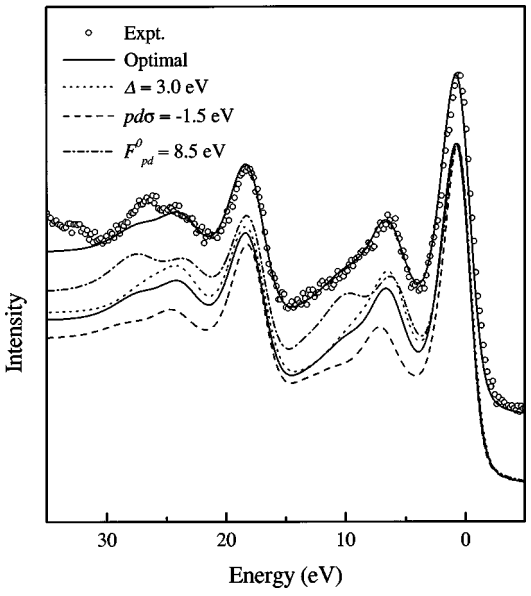

FIG. 4. Experimental Ni $2p$ core-level spectrum (open circles) of Lu_2BaNiO_5 along with the simulated spectra for various parameter strengths. The solid line is calculated with the optimum parameter set, as described in the text. The dotted line shows the spectrum corresponding to $\Delta=3.0$ eV with all other parameters remaining unchanged. The dashed line and the dot-dashed line represent the spectra corresponding to $pd\sigma=-1.5$ eV and $F^0_{pd}=8.5$ eV, respectively.

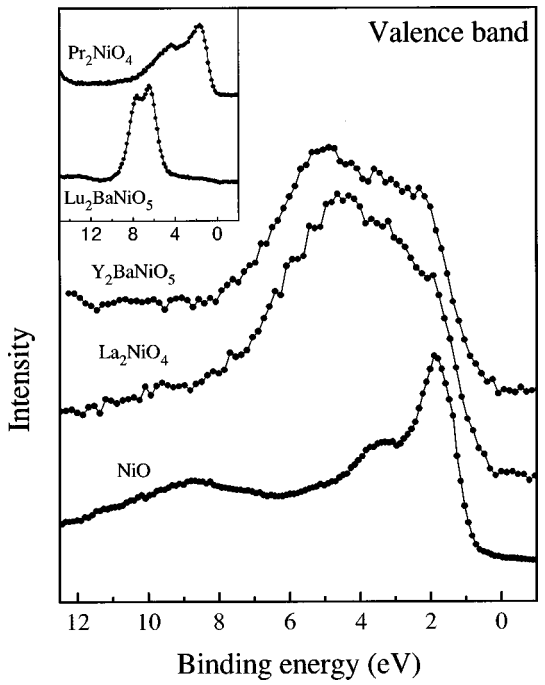

FIG. 5. Valence-band spectra of NiO, La_2NiO_4, and Y_2BaNiO_5. The spectrum corresponding to NiO has been adopted from the literature (Ref. 42). The inset shows the valence-band spectra of Pr_2NiO_4 and Lu_2BaNiO_5 demonstrating the dominance of the $4f$ signals of the rare-earth elements involved in the compounds.

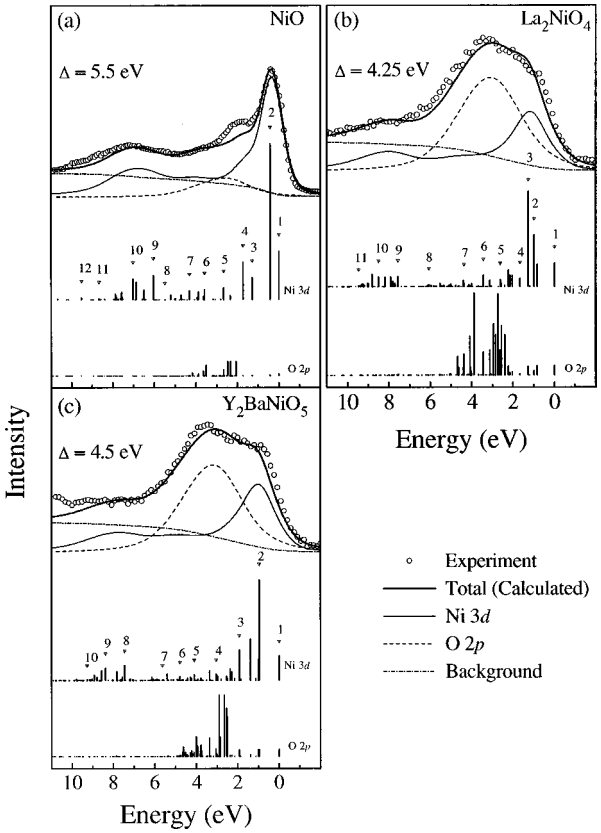

FIG. 6. Comparison of the experimental (open circles) and the calculated (thick lines) valence-band spectra of (a) NiO; (b) La_2NiO_4; and (c) Y_2BaNiO_5. The contributions from Ni $3d$ (thin lines), O $2p$ (dashed line), and the inelastic background (dotted lines) to the total calculated spectra are also shown along with the corresponding bar diagrams obtained from the cluster calculations. The numbers mark the energies where an analysis of the character of the final-state wave functions were carried out and the corresponding results are given in the Tables V–VII.

clear from the inset that the signals corresponding to the Ni $3d$ and O $2p$ photoemissions are almost completely smeared out due to the overlap of the large intensity of $4f$ signals arising from the rare-earth elements (Pr and Lu) present in these two samples, and therefore precludes any quantitative analysis. All the spectra are normalized at the energy position of the Ni $3d$ peak manifested in the photoemission spectrum of NiO. The energy region 1–4 eV binding energies is primarily dominated by the Ni $3d$ related features and the oxygen $2p$ contributions appear at higher energies. The analysis of the valence-band spectra with various photon energies in the case of Y_2BaNiO_5[39] and La_2NiO_4[28] shows that the intense feature around 5 eV binding energy is dominated by the photoemission from the bonding levels with large oxygen $2p$ character and the feature at about 3.5 eV binding energy are related to primarily oxygen levels with a nonbonding character with respect to Ni d- O p interactions. The broad and intense feature in the energy range 8–10 eV has been interpreted as correlation induced satellites associated with the photoemission of Ni $3d$ states.

In order to provide a quantitative analysis of the features in the valence-band photoemission spectrum of NiO, we have calculated the same within the cluster model that was also used for the calculation of the core-level spectrum. It is well known[24] that the valence band and the core-level spectra often require slightly different sets of parameter strengths, such as the charge-transfer energy and the electron-electron interaction strengths. In the core-level spectral simulation, we used only two parameters Δ and F^0_{pd} as adjustable ones, in order to minimize the number of free parameters. In the same spirit, we use Δ as the single adjustable parameter for calculating the valence band spectra. It turns out that a good description of the NiO valence band experimental spectrum is obtained with the multiplet averaged charge-transfer energy Δ being equal to 5.5 eV, which is the same as that obtained from the core-level calculation [see Fig. 3(a)]. This provides further credence to the reliability of the estimates of charge-transfer energy obtained in the present paper. We plot the calculated spectrum (thick solid line) compared to the experimental spectrum (open circles) in Fig. 6(a). The total calculated spectrum is composed of the contributions arising from the Ni $3d$ photoemission (thin solid line), the O $2p$ photoemission (dashed line) *both calculated within the same model*, and a smoothly varying integral background function (short dash) to account for the inelastic scattering of the photoemitted electrons. As is evident from the comparison in Fig. 6(a), the calculated spectrum provides a good description of the experimental one over the entire energy range, except for some underestimation of the intensity at about 2 eV. Most of the distinct spectral features arise from the Ni $3d$ photoemission contributions (the thin line), which provide a particularly good agreement for the spectral regions near the main peak and the satellite regions. The oxygen $2p$ photoemission contributions provide a featureless broad intensity between about 0 and 5 eV, with a peak at about 2.2 eV. Since we use exactly the same parameter set here, as in the core-level calculation for NiO, the description of the ground-state wave function remains identical between the two cases. We show the character of the various final states responsible for different features in the spectrum in Table V. It is evident from this table that the lowest energy excitations

TABLE V. Contributions of various configurations in the final state of valence-band photoemission in NiO.

Peak no.	1	2	3	4	5	6	7	8	9	10	11	12
Energy	0.0	0.41	1.28	1.72	2.66	3.57	4.31	5.49	6.05	7.03	8.67	9.52
d^7	21.86	37.98	23.85	24.61	0	8.62	6.59	2.32	39.50	43.13	58.51	67.33
$d^8\underline{L}$	64.66	54.93	66.31	64.62	91.62	81.33	87.89	90.14	48.51	32.14	27.06	8.96
$d^9\underline{L}^2$	13.11	6.98	9.69	10.58	8.38	10.00	5.48	7.48	11.74	23.16	14.17	23.07
$d^{10}\underline{L}^3$	0.37	0.11	0.15	0.19	0	0.05	0.04	0.06	0.25	1.57	0.26	0.64

TABLE VI. Contributions of various configurations in the final state of valence-band photoemission in La_2NiO_4.

Peak no.	1	2	3	4	5	6	7	8	9	10	11
Energy	0.0	0.98	1.28	1.67	2.62	3.44	4.38	6.08	7.56	8.50	9.46
d^7	16.41	27.18	16.92	18.27	4.09	0	0.35	1.87	55.58	50.60	58.72
$d^8\underline{L}$	63.31	60.43	66.48	66.60	75.46	89.52	83.90	82.28	15.65	24.20	11.67
$d^9\underline{L}^2$	19.48	12.09	16.23	14.75	19.83	10.48	15.51	15.58	27.43	23.98	28.64
$d^{10}\underline{L}^3$	0.80	0.31	0.37	0.39	0.61	0	0.24	0.27	1.34	1.22	0.97

in the valence band [marked 1–4 in Fig. 6(a)] corresponding to the main peak are dominated by the $d^8\underline{L}^1$ configuration with a substantial contribution ($\sim$22–38 %) from the d^7 configuration. In contrast, the weaker intensity feature (marked 5–8) between 2–5.5 eV have almost purely $d^8\underline{L}^1$ character with little contribution from all the other configurations. The O $2p$ photoemission contribution is also observed precisely in this range of energies consistent with the experimental results with lower photon energies.[59] The satellite feature spanning the energy interval 6–10 eV [marked 9–12 in Fig. 6(a)] has a dominant contribution from the d^7 configuration with nonnegligible contributions from $d^8\underline{L}^1$ and $d^9\underline{L}^2$ configurations; these results are similar with earlier interpretations.[12,24]

Now we turn to the valence-band spectrum of two-dimensional nickelates. As we have already pointed out, it is not possible to analyze the valence-band spectrum of Pr_2NiO_4 due to the interference from the Pr $4f$ signals. Instead, we analyze the valence-band spectrum of La_2NiO_4, as a representative case of the two-dimensional electronic structure. In order to simulate the valence-band spectrum of La_2NiO_4 with Δ as the only adjustable parameter, we find that it is not possible to provide a proper description with the Δ value that was used for the core-level calculation of the other two-dimensional nickelate Pr_2NiO_4. Instead, it was found that a somewhat larger Δ ($=4.25$ eV) is required to simulate the experimental spectrum. We show the resulting calculated spectrum (thick line) in comparison to the experimental one (open circles) along with the individual Ni $3d$ (thin line) and O $2p$ (dashed line) contributions in Fig. 6(b). It is to be noted here that the contribution of the O $2p$ states in the valence-band spectrum of La_2NiO_4 is considerably larger compared to that in NiO, arising from the much larger O to Ni atomic ratio in La_2NiO_4. While the Δ value is larger than that used for Pr_2NiO_4 core-level spectral simulations, it is significantly smaller than that ($\Delta=5.5$ eV) in three-dimensional NiO. It is evident from the comparison in Fig. 6(b) that the calculated spectrum provides excellent agreement over the entire energy range up to about 11 eV. The calculated spectrum of the Ni $3d$ states shows the dominant contribution around 0–2 eV with weak intensities distributed in the higher energy regions. The spectral intensity in the energy range 3–7 eV is primarily due to the photoemission from the oxygen $2p$ states with small contributions from Ni $3d$ states. This result is consistent with the experimental observations concerning the changes in the spectral intensities with different photon energies.[28] There is a distinct satellite feature in the energy range 7–10 eV contributed almost entirely by the Ni $3d$ photoemissions. This satellite feature has much lower intensity compared to that in NiO. The parameters simulating the spectra of La_2NiO_4 and NiO suggest that this reduction in the satellite intensity primarily arises from the reduction in the Δ value leading to an increased covalency that transfers spectral weight to better screened final states. In this case, the ground-state wave function contains about 77%, 22%, and 1% of d^8, $d^9\underline{L}^1$, and $d^{10}\underline{L}^2$ configurations, respectively, with a corresponding total $3d$ occupancy n_d equal to 8.23. These results indeed show that La_2NiO_4 is more mixed valent due to the increased covalency compared to NiO. The character of the spectral features appearing at different energy regions are tabulated in terms of various configurations in Table VI; the qualitative trend here is similar to that in NiO (Table V). The 0–2 eV energy region [marked 1–4 in Fig. 6(b)] is primarily contributed by the $d^8\underline{L}^1$ configuration with an admixture (15–20 %) of the d^7 and $d^9\underline{L}^2$ configurations. An increased contribution from the $d^9\underline{L}^2$ configuration to this energy region corresponding to the leading spectral features in La_2NiO_4 compared to that in NiO (see Table V), is due to the increased stability of the $d^9\underline{L}^2$ state in La_2NiO_4 as a consequence of the lower Δ value. The Ni $3d$ photoemission contribution has nearly pure $d^8\underline{L}^1$ character in the energy range 3.5–7 eV with negligible contribution from other configurations. The spectrum in this range is entirely dominated by the photoemission contribution from O $2p$ states, as shown in the figure. The satellite region (7–10 eV) is dominated by the d^7 configuration ($\sim$50%) as expected.

The valence-band spectrum of one-dimensional Y_2BaNiO_5 is shown in Fig. 6(c). While the first 10 eV of the spectrum is contributed almost entirely by Ni $3d$ and O $2p$ states, the rising spectral signature beyond 10 eV arises from the photoemission signal from Ba $5p$ levels appearing at higher energies.[39] In order to provide a reasonable description of the experimental spectrum in terms of the calculated spectrum, it was found necessary to use a value of Δ somewhat larger than the one estimated from the core-level analysis. In the present case, $\Delta=4.5$ eV provides a reasonable description of the valence-band photoemission spectrum from Y_2BaNiO_5. We show the comparison between the experimental spectrum and the calculated one along with the calculated Ni $3d$ and O $2p$ contributions in Fig. 6(c). As in the other cases, the calculated spectrum provides a reliably accurate description of the experimental one. This value of Δ along with the other parameter strengths characterizes the ground state as 80%, 20%, and 1% of the d^8, $d^9\underline{L}^1$, and $d^{10}\underline{L}^2$ configurations, respectively, resulting in an n_d of 8.21. The characters of different spectral features are tabulated in

TABLE VII. Contributions of various configurations in the final state of valence-band photoemission in Y_2BaNiO_5.

Peak no.	1	2	3	4	5	6	7	8	9	10
Energy	0.0	0.96	2.54	3.04	4.09	4.79	6.10	7.46	8.38	9.49
d^7	18.04	28.80	2.46	0.03	2.05	2.21	4.23	45.68	43.36	48.51
$d^8\underline{L}$	63.67	59.94	78.56	85.95	82.18	87.21	81.64	31.08	19.58	17.23
$d^9\underline{L}^2$	17.67	11.00	18.48	14.02	15.67	10.39	13.88	22.45	34.35	33.27
$d^{10}\underline{L}^3$	0.65	0.25	0.51	0	0.11	0.19	0.26	0.79	2.71	1.00

Table VII and are similar to those in La_2NiO_4.

Electronic structure of transition metal compounds has been categorized[60–62] in terms of the well-known Zaanen-Sawatzky-Allen phase diagram based on the relative strengths of U, Δ, and t_{dp}. In the insulating regime of large Δ and U, $\Delta > U$ characterizes a Mott-Hubbard insulator, while one obtains a charge-transfer insulator in the opposite limit $U > \Delta$. It has been pointed out earlier[12,13] that NiO is characterized by $U \geqslant \Delta$, which is in agreement with the present finding. This places NiO close to the boundary region between the charge-transfer insulators and Mott-Hubbard insulators; this has led to the classification of NiO as an insulator with mixed character. We find that Δ decreases rapidly across the series with decreasing dimensionality, suggesting a more pronounced charge-transfer insulator character for the compounds with lower dimensional crystal structure. Zero-dimensional Lu_2BaNiO_5 with $U_{dd} = 6.52$ eV and $\Delta = 2.5$ eV clearly belongs to the charge-transfer limit. We investigate the changes in the value of Δ and n_d in Fig. 7. The open symbols denote the values of n_d and the solid symbols show the Δ values. The triangles in the figure represent the estimates from the valence-band calculations and the circles represent those from the Ni $2p$ core level calculations. While the electron-electron interaction parameters, namely F^0_{dd} (=7 eV), F^2_{dd} (=9.175 eV), F^4_{dd} (=5.698 eV), F^2_{pd} (=5.791 eV), G^1_{pd}(=4.341 eV), and G^3_{pd} (=2.468 eV) were kept fixed for all the compounds and the hopping interaction strengths were obtained by scaling a single set of $(pd\sigma)$, $(pd\pi)$, $(pp\sigma)$, and $(pp\pi)$ with the Ni-O and O-O distances, the figure clearly shows that Δ reduces with the decrease in dimensionality with a concomitant increase in the values of n_d. The charge-transfer energy Δ can be expressed as,

$$\Delta = E(d^{n+1}\underline{L}^1) - E(d^n) = \epsilon_d - \epsilon_p + nU_{dd}.$$

Thus, U_{dd} being unchanged across the series, the change in Δ is primarily related to the change in $(\epsilon_d - \epsilon_p)$, the bare-energy difference. The value of this term besides depending on the atomic potentials, is influenced considerably by the crystal lattice potential.

In order to investigate the role of Madelung potential on the charge-transfer energy, we have calculated the Madelung potential for each of the cases studied here. The charge-transfer energy is related to the difference in Madelung potentials at Ni and oxygen sites (ΔV_M).[63] Following Ref. 64, ΔV_M can be computed for a given lattice under the assumption of fully ionized atomic sites (ionic limit) in the lattice. This way, we obtain the value of ΔV_M for three-dimensional NiO, to be 48.36 eV. The values of ΔV_M in two-dimensional La_2NiO_4 range between 48.62 and 49.48 eV arising from nonequivalent oxygen sites in this compound. ΔV_M is somewhat smaller (48.14–49.08 eV) in one-dimensional Y_2BaNiO_5; there is a further decrease to 46.14–47.09 eV for zero-dimensional Lu_2BaNiO_5. Thus, the overall decreasing trend in Δ with decreasing dimensionality follows the trend obtained in ΔV_M in these compounds, except only for the case of NiO. It is important to note here that, the values of ΔV_M are calculated assuming ionic configurations of all the elements in the solid and it is possible that a more accurate determination of this quantity including the true charge states may account for the case of NiO also. This is indicated by the fact that NiO has the most ionic ground state among all the compounds studied here; this should in general enhance ΔV_M for NiO compared to the other compounds.

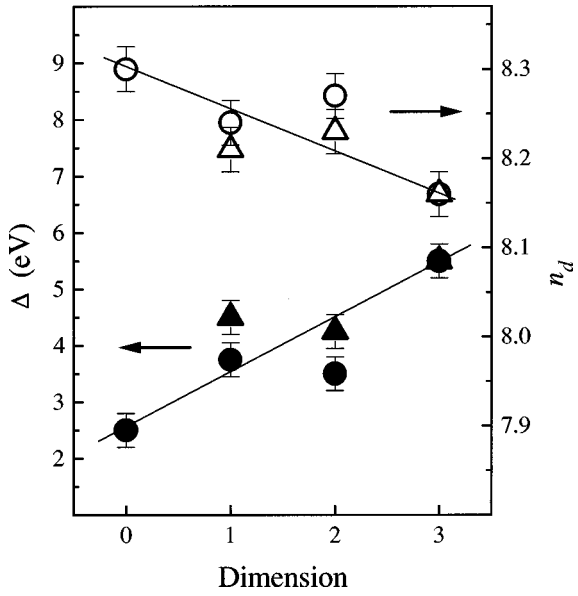

FIG. 7. The charge-transfer energy $\triangle$ (solid symbols) and total $3d$ electron counts, n_d (open symbols) are plotted as a function of the dimensionality of the Ni-O-Ni network. The triangles are the estimations from valence-band calculations and the circles are those from the Ni $2p$ photoemission calculations.

VI. CONCLUSIONS

In conclusion, we provide a detailed study of the electronic structure of divalent nickelates with different dimensionality (Ni-O-Ni connectivity). The electronic structures of these compounds exhibit substantial changes with the change

in the dimensionality. We analyzed the electronic spectra within the cluster approximation *evaluating both Ni* $3d$ *and O* $2p$ *contributions on the same footing*, thereby providing a quantitative description of the electronic structure in each case. It is found that the changes in the electronic structure are primarily due to a systematic variation in the charge-transfer energy (Δ). Since the effective coupling between the Ni sites determining the $3d$ bandwidth is controlled by Ni-O-Ni hoppings, a reduction of the dimensionality is expected to reduce the bandwidth; on the other hand, a concomitant reduction in the charge-transfer energy Δ, enhancing the effective coupling between the Ni sites at least partially compensates the bandwidth reduction. Moreover, a change in Δ directly influences the band gap within the charge-transfer regime. The change in Δ is primarily related to changes in $(\epsilon_d - \epsilon_p)$, the bare energy difference due to changes in the Madelung potential. Another important consequence of decreasing Δ is to increase the average $3d$ occupancy n_d, with decreasing dimensionality in these divalent nickelates. This change in Δ is also responsible for changing the character of the satellite feature in the core-level photoemission from a primarily poorly screened d^8 state in NiO to a dominantly *overscreened* $d^{10}\underline{L}^2$ state in the compounds with lower dimensional Ni-O-Ni networks. The results clearly establish a systematic undermining of the influence of the nonlocal screening channel on the spectral shape with decreasing Ni-O-Ni connectivity and provide a suitable testing ground for more rigorous theoretical treatments within the multi-impurity models to unravel the nature and origin of nonlocal screening dynamics in transition metal oxides.

ACKNOWLEDGMENTS

The authors thank Professor C. N. R. Rao for continued support and the Department of Science and Technology, Government of India, for financial support. K.M. and P.M. thank the Council of Scientific and Industrial Research, Government of India, for financial assistance. The authors also thank Professor S. Ramasesha and the Supercomputer Education and Research Center, Indian Institute of Science, for providing the computational facility.

*Also at Department of Physics, Indian Institute of Science, Bangalore, India.

†Also at Condensed Matter Theory Unit, Department of Physics, Indian Institute of Science and Jawaharlal Nehru Center of Advanced Scientific Research, Bangalore, India. Electronic address: sarma@sscu.iisc.ernet.in

[1] N. F. Mott, *Metal Insulator Transitions*, 2nd ed. (Taylor & Francis, London, 1990).

[2] J. Hubbard, Proc. R. Soc. London, Ser. A **276**, 238 (1963); **277**, 237 (1964); **281**, 401 (1964).

[3] R. von Helmolt *et al.*, Phys. Rev. Lett. **71**, 2331 (1993); S. Jin *et al.*, Science **264**, 413 (1994).

[4] G. Bednorz and K. A. Muller, Z. Phys. B **64**, 189 (1986).

[5] K. Maiti, D. D. Sarma, T. Mizokawa, and A. Fujimori, Phys. Rev. B **57**, 1572 (1998); Europhys. Lett. **37**, 359 (1997).

[6] F. Marabelli, G. B. Parravicini, and F. Salghetti-Drioli, Phys. Rev. B **52**, 1433 (1995).

[7] S. L. Cooper, G. A. Thomas, A. J. Millis, P. E. Sulewski, J. Orenstein, D. H. Rapkine, S.-W. Cheong, and P. L. Trevor, Phys. Rev. B **42**, 10 785 (1990).

[8] Y. Tokura, S. Koshihara, T. Arima, H. Tagaki, S. Ishibashi, T. Ido, and S. Uchida, Phys. Rev. B **41**, 11 657 (1990).

[9] T. Mizokawa *et al.*, Phys. Rev. Lett. **67**, 1638 (1991).

[10] S. Nimkar, D. D. Sarma, and H. R. Krishnamurthy, Phys. Rev. B **47**, 10 927 (1993).

[11] D. D. Sarma, Rev. Solid State Sci. **5**, 461 (1991).

[12] A. Fujimori, F. Minami, and S. Sugano, Phys. Rev. B **29**, 5225 (1984).

[13] A. Fujimori and F. Minami, Phys. Rev. B **30**, 957 (1984).

[14] D. D. Sarma and A. Taraphder, Phys. Rev. B **39**, 11 570 (1989).

[15] M. A. van Veenendaal and G. A. Sawatzky, Phys. Rev. Lett. **70**, 2459 (1993).

[16] M. A. van Veenendaal and G. A. Sawatzky, Phys. Rev. B **47**, 11 462 (1993).

[17] M. A. van Veenendaal, H. Eskes, and G. A. Sawatzky, Phys. Rev. B **49**, 3473 (1994).

[18] K. Okada and A. Kotani, J. Electron Spectrosc. Relat. Phenom. **78**, 53 (1996).

[19] K. Okada, A. Kotani, K. Maiti, and D. D. Sarma, J. Phys. Soc. Jpn. **65**, 1844 (1996).

[20] K. Terakura, A. R. Williams, and J. Kübler, Phys. Rev. B **30**, 4734 (1084).

[21] G. A. Sawatzky and J. W. Allen, Phys. Rev. Lett. **53**, 2339 (1984).

[22] L. F. Mattheiss, Phys. Rev. B **5**, 290 (1972).

[23] Manabu Takahashi and Jun-ichi Igarashi, Ann. Phys. **5**, 247 (1996); Phys. Rev. B **54**, 13 566 (1996).

[24] M. A. van Veenendaal, *The Theory of Core-Level Line Shapes Beyond The Impurity Limit*, Ph.D. thesis, University of Groningen, 1994.

[25] J. D. Jorgensen, B. Dabrowski, Shiyou Pei, D. R. Richards, and D. G. Hinks, Phys. Rev. B **40**, 2187 (1989).

[26] Priya Mahadevan, K. Sheshadri, D. D. Sarma, H. R. Krishnamurthy, and Rahul Pandit, Phys. Rev. B **55**, 9203 (1997).

[27] P. Kuiper, J. van Elp, G. A. Sawatzky, A. Fujimori, S. Hosoya, and D. M. de Leeuw, Phys. Rev. B **44**, 4570 (1991).

[28] H. Eisaki, S. Uchida, T. Mizokawa, H. Namatame, A. Fujimori, J. van Elp, P. Kuiper, G. A. Sawatzky, S. Hosoya, and H. Katayama-Yoshida, Phys. Rev. B **45**, 12 513 (1992).

[29] G. Y. Guo and W. M. Temmerman, Phys. Rev. B **40**, 285 (1989); J. Phys. C **21**, L917 (1988).

[30] J. B. Grant and A. K. McMahan, Physica C **162-164**, 1439 (1989).

[31] E. Pellegrin, J. Zaanen, H.-J. Lin, G. Meigs, C. T. Chen, G. H. Ho, H. Eisaki, and S. Uchida, Phys. Rev. B **53**, 10 667 (1996).

[32] S. C. Chen, K. V. Ramanujachary, and Martha Greenblatt, Solid State Chem. **105**, 444 (1993).

[33] D. J. Buttrey, J. D. Sullivan, G. Shirane, and K. Yamada, Phys. Rev. B **42**, 3944 (1990).

[34] J. A. Alonso, I. Rasines, J. Rodríguez-Carvajal, and J. B. Torrance, Solid State Chem. **109**, 231 (1994); J. Amador, E. Gutiérrez-Puebla, M. A. Monge, I. Rasines, C. Ruiz-Valero, F. Fernández, R. Saez-Puche, and J. A. Campá, Phys. Rev. B **42**, 7918 (1990).

[35] J. F. DiTusa, S-W. Cheong, J.-H. Park, G. Aeppli, C. Broholm, and C. T. Chen, Phys. Rev. Lett. **73**, 1857 (1994).

[36] F. D. M. Haldane, Phys. Lett. A **93**, 464 (1983); Phys. Rev. Lett. **50**, 1153 (1983).
[37] J. Darriet and L. P. Regnault, Solid State Commun. **86**, 409 (1993).
[38] J. F. DiTusa, S-W. Cheon, J.-H. Park, G. Aeppli, C. Broholm, and C. T. Chen, Phys. Rev. Lett. **73**, 1857 (1994).
[39] K. Maiti and D. D. Sarma, Phys. Rev. B **58**, 9746 (1998).
[40] Hk. Müller-Buschmaum and I. Rüter, Z. Anorg. Allg. Chem. **572**, 181 (1989).
[41] J. A. Alonso, I. Rasines, J. Rodríguez-Carvajal, and J. B. Torrance, Solid State Chem. **109**, 231 (1994).
[42] S. P. Kowalczyk, L. Ley, R. A. Pollack, and D. A. Shirley, as cited in J. H. Brandow, Adv. Phys. **26**, 651 (1977).
[43] F. M. F. de Groot, J. C. Fuggle, B. T. Thole, and G. A. Sawatzky, Phys. Rev. B **42**, 5459 (1990).
[44] G. van der Laan and I. W. Kirkman, J. Phys.: Condens. Matter **4**, 4189 (1992).
[45] J. Zaanen, G. A. Sawatzky, J. Fink, W. Speier, and J. C. Fuggle, Phys. Rev. B **32**, 4905 (1985).
[46] J. C. Slater and G. F. Koster, Phys. Rev. **94**, 1498 (1954).
[47] Walter A. Harrison, *Electronic Structure and the Properties of Solids, The Physics of the Chemical Bond* (Dover, New York, 1989).
[48] Carl J. Ballhausen, *Introduction to Ligand Field Theory* (McGraw-Hill, New York, 1962).
[49] E. Dagotto, Rev. Mod. Phys. **66**, 763 (1994).
[50] D. D. Sarma, F. U. Hillebrechet, W. Speier, N. Mårtensson, and D. D. Koelling, Phys. Rev. Lett. **57**, 2215 (1986).
[51] W. Speier, E. V. Leuken, J. C. Fuggle, D. D. Sarma, L. Kumar, B. Dauth, and K. H. Buschow, Phys. Rev. B **39**, 6008 (1988).
[52] J. J. Yeh and I. Lindau, At. Data Nucl. Data Tables **32**, 1 (1985).
[53] G. A. Sawatzky and D. Post, Phys. Rev. B **20**, 1546 (1979).
[54] T. Böske, K. Maiti, O. Knauff, K. Ruck, M. S. Golden, G. Krabbes, J. Fink, T. Osafune, N. Motoyama, H. Eisaki, and S. Uchida, Phys. Rev. B **57**, 138 (1998).
[55] J. Zaanen and G. A. Sawatzky, Phys. Rev. B **33**, 8074 (1986).
[56] D. D. Sarma, J. Phys. Soc. Jpn. **65**, 1325 (1996).
[57] K. Maiti and D. D. Sarma, Phys. Rev. B **54**, 7816 (1996).
[58] B. E. F. Fender, A. J. Jacobson, and F. A. Wedgewood, J. Chem. Phys. **48**, 990 (1968).
[59] J. M. McKay and V. E. Henrich, Phys. Rev. Lett. **53**, 2343 (1984).
[60] J. Zaanen, G. A. Sawatzky, and J. W. Allen, Phys. Rev. Lett. **55**, 418 (1985).
[61] D. D. Sarma, Seva Nimkar, H. R. Krishnamurthy, and T. V. Ramakrishnan, Pramana, J. Phys. **38**, L531 (1992).
[62] Seva Nimkar, D. D. Sarma, H. R. Krishnamurthy, and S. Ramasesha, Phys. Rev. B **48**, 7355 (1993).
[63] Y. Ohta, T. Tohyama, and S. Maekawa, Phys. Rev. Lett. **66**, 1228 (1991); Phys. Rev. B **43**, 2968 (1991).
[64] J. B. Torrance, P. Lacorre, C. Asavaroengchai, and M. Metzger, Physica C **182**, 351 (1991).